Coarse graining atomistic simulations of plastically deforming amorphous solids

Adam R. Hinkle,[1] Chris H. Rycroft,[2] Michael D. Shields,[1,3] and Michael L. Falk[1,4,5]
[1]*Department of Materials Science & Engineering, Johns Hopkins University, Baltimore, Maryland 21218, USA*
[2]*Paulson School of Engineering & Applied Sciences, Harvard University, Cambridge, Massachusetts 02138, USA*
[3]*Department of Civil Engineering, Johns Hopkins University, Baltimore, Maryland 21218, USA*
[4]*Department of Mechanical Engineering, Johns Hopkins University, Baltimore, Maryland 21218, USA*
[5]*Department of Physics & Astronomy, Johns Hopkins University, Baltimore, Maryland 21218, USA*
(Received 8 January 2017; published 5 May 2017)

The primary mode of failure in disordered solids results from the formation and persistence of highly localized regions of large plastic strains known as shear bands. Continuum-level field theories capable of predicting this mechanical response rely upon an accurate representation of the initial and evolving states of the amorphous structure. We perform molecular dynamics simulations of a metallic glass and propose a methodology for coarse graining discrete, atomistic quantities, such as the potential energies of the elemental constituents. A strain criterion is established and used to distinguish the coarse-grained degrees-of-freedom inside the emerging shear band from those of the surrounding material. A signal-to-noise ratio provides a means of evaluating the strength of the signal of the shear band as a function of the coarse graining. Finally, we investigate the effect of different coarse graining length scales by comparing a two-dimensional, numerical implementation of the effective-temperature description in the shear transformation zone (STZ) theory with direct molecular dynamics simulations. These comparisons indicate the coarse graining length scale has a lower bound, above which there is a high level of agreement between the atomistics and the STZ theory, and below which the concept of effective temperature breaks down.

DOI: 10.1103/PhysRevE.95.053001

I. INTRODUCTION

Amorphous solids are characterized by a complex, random arrangement of their atomic or molecular constituents [1–3]. While amorphous materials have long presented a great scientific challenge due to the nature of their disordered structure, significant progress has been made toward a theoretical foundation relating the degree of disorder of the solid to thermodynamic principles [4–7]. Amorphous solids are essentially indistinguishable from fluids in their microscopic structure, but they are unlike fluids in that they exhibit a yield stress below which they respond elastically to external forces, while fluids flow even under infinitesimal shear stresses. Once an amorphous solid is subjected to a shear stress that exceeds the yield stress, it can flow plastically in a manner that depends on the temperature, the shear-rate, and the density [8]. Microscopically, the plastic flow is widely believed to arise from local rearrangements of the constituents in response to these external conditions, and in recent years a proliferation of many distinct theoretical models characterizing these rearrangements in different ways has occurred [9–22]. The most appropriate way to build a physical connection between the amorphous microstructure and the observed mechanical response such as shear banding, a critical failure mode in many amorphous materials, remains controversial.

Shear banding, as the name implies, is a plastic instability that localizes large shear strains in a relatively thin band when a material is deformed [23]. A shear band has the ability to broaden and invade the surrounding material outside the band, which remains nearly undeformed [24–26]. Shear bands have been widely observed in metals, polymers, the Earth's mantle, granular solids, yield stress fluids, and many other materials, including liquids under shear flow [27]. In metallic glasses, shear banding is the primary mode of deformation, from yielding to failure. One specific attempt to link local particle rearrangements to shear banding is the shear transformation zone (STZ) theory [4–7,28,29], which proposes that zones of tens or even hundreds of particles undergo transitions between two states resulting in an increment of plastic strain. The STZ theory is distinct from other approaches in that a constitutive law relates the transitions to an effective temperature [30–38], describing the deforming amorphous structure in terms of a continuum field. A mathematical field theory of this kind has significant advantages as it essentially reduces the particle-level complexity of amorphous plasticity to a boundary-value problem in solid mechanics, but with the challenge of generating appropriate initial conditions, determining values of the theory's physical parameters, and establishing an accurate method of validation.

Related to these considerations is the notion that a well-formulated continuum theory must have far fewer degrees-of-freedom (DOF) than, for example, detailed atomistic simulations, and should also provide a computationally efficient description of the mechanical response. In particular, it would make the continuum assumption that a representative volume element (RVE) exists. The RVE has been defined as the smallest material volume element of the system for which the usual spatially constant macroscopic constitutive representation is a sufficiently accurate model to represent mean constitutive response [39]. This continuum assumption is equivalent to neglecting the local heterogeneity of the stresses and strains within the RVE, and instead working with averaged quantities, as the effects of the heterogeneities act only indirectly through a certain number of internal variables [40]. For crystalline materials a great number of methods have been constructed using the continuum hypothesis to describe elastoplastic behavior, including nonlocal, energy-based, and multiscale frameworks [40,41].

The procedure of selectively reducing the number of DOF of a system, known as coarse graining, is essential to constructing a predictive continuum-level description. However, differences in system complexity and purpose of modeling often lead to difficulties in developing a universal method for coarse graining [42]. Attempts to formulate generalized coarse graining frameworks, which account for a wide range of physical phenomena (e.g., elasticity and electrical conductivity) often result in a complex coarse graining procedure with large numbers of parameters and a diminished representation compared to frameworks following a phenomena-dependent focus. Several rigorous methods have been developed for equilibrium systems where there is a well-defined partition function [43,44]. In cases where the system is driven out of equilibrium, e.g., through the process of shear, such clear statistical mechanics-based descriptions are often precluded or extremely difficult to formulate.

Earlier work has attempted to address the problem of coarse graining the amorphous microstructure by constructing so-called "mesoscale models" that connect the original STZ transition-rate equations to finite element calculations [17,45,46] and evolving the system using either a kinetic Monte Carlo or an extremal dynamics algorithm. Similar techniques have been applied to three-dimensional systems [47] and connections to the realistic timescales of experiments have been made. Lattice-based depinning models have been proposed, which describe plasticity in amorphous solids by allowing local element interfaces to slip in a random fashion [48–51]. Significant limitations exist with these mesoscale approaches. For amorphous solids in particular, the nature of the RVE has not been well investigated and remains largely unknown. In nearly all mesoscale models the RVE is merely taken to be the size of an individual STZ or slip event, and so the fundamental question regarding how to correctly average over experimental or atomistic data of the amorphous microstructure has not been addressed. Moreover these approaches have no connection to fundamental thermodynamic considerations, which are known to be essential in describing the shear-induced disordering of the material's structure during plastic deformation [52]. This is most apparent in that changes in energy between material states of varying disorder are typically not quantified in these models, and energetic criteria play no role in influencing transition rates. Furthermore, only rather modest and tangential comparisons to experiments and atomistic simulations using these techniques have been attempted so far, usually in the form of a demonstration that the model can produce some feature of the deformation qualitatively, such as the presence of a yield stress or a stress-strain history that is typical of a metallic glass.

In contrast to much of the prior work, we approach the problem of coarse graining by translating details directly from an amorphous system where atom-by-atom information is known and accessible. This is distinct from building a coarse-grained representation from an established set of assumptions. In choosing to directly reduce the number of DOF in this way, we are able to recast the problem as a study of averages of atomic-level quantities over some chosen length scale. Because changes in atomic potential energy reflect changes in the amorphous structure [53], we believe it is important to study the statistics of these energies, how these statistics evolve as the material is driven out of equilibrium during shear, and how the statistics depend on the size of the RVE (i.e., coarse graining length scale). Of paramount importance is understanding whether there is an optimal coarse graining length scale for these quantities such that the shear banding and the mechanical response is best captured when cross-comparisons are made between the coarse-grained atomistics and a continuum description. In this paper we propose a methodology for coarse graining discrete, atomistic data pertaining to an amorphous solid, and use the coarse-grained representations to initialize and validate the effective-temperature dynamics of the STZ theory. Specifically, we preform molecular dynamics (MD) simulations of amorphous copper-zirconium (CuZr) under simple shear, and then coarse-grain the MD system for a range of length scales to obtain continuum representations of potential energy and atomic strain.

The structure of this paper is as follows. In Sec. II we present the details of the coarse graining methodology devised to efficiently take advantage of the detailed per-atom information of the MD simulations. Then in Sec. III we define a *signal* of the shear band and distingish it from the *background* through a criterion that connects the atomic strain to the potential energy. Analysis of the system's signal-to-noise suggests a lower bound on the coarse graining length scale. In Sec. IV we apply the coarse graining procedure to the MD system and extract an initial condition for the effective-temperature field in the STZ theory. We compare the coarse-grained MD simulation of the shear banding alongside the results of a two-dimensional, quasi-static numerical implementation of STZ theory using this initial condition. We conclude in Sec. V with a discussion of how this preliminary work can inform future efforts to develop continuum theories of amorphous plasticity where coarse-grained representations of atomistic data are used to parametrize and validate the material models.

II. COARSE-GRAINING METHODOLOGY

MD simulations were preformed using the LAMMPS software [54] with a well-established embedded-atom-method (EAM) interaction potential [55]. The initial presheared glass was formed by taking a 50-50 composition of CuZr with 297,680 total atoms and quenching the equilibrated liquid at a rate of 10^{11} K/s to a temperature $T = 100$ K. The system is square with sides of length $L = 400$ Å, and has a thin out-of-plane direction (30 Å) that allows us to treat the system as effectively two-dimensional. A nonequilibrium molecular dynamics (NEMD) shear simulation was preformed by deforming the simulation box of the quenched glass under simple shear conditions at constant volume and temperature with periodic boundary conditions in all directions enforced by the SLLOD [56] equations of motion. A time step of 0.005 picoseconds (ps) and an applied shear rate $\dot{\gamma} = 10^{-4}$ ps^{-1} were used. The system was held at 100 K for the duration of the shear. The NEMD shear simulation revealed the formation of a shear band near the center of the simulation box. The shear band was aligned with the direction of shear and continued to broaden as the system was deformed.

The corresponding coarse-grained representation of the system is defined by a two-dimensional square grid of equally

spaced continuum points. We map the the atomic potential energies to the grid using a Gaussian function $g_n = g(r_n,c)$ of the form

$$g_n = \frac{2}{\sqrt{2\pi}c}\exp\left(-\frac{r_n^2}{2c^2}\right) \quad (1)$$

to weight the contributions of each atom. The function g_n is centered on continuum point α and r_n is the distance from α to atom-n and defines a coarse-grained region determined by the cutoff radius r_{cut}. In this way, neighboring regions are allowed to overlap with one another. The coarse-grained atomic potential energy E_α at α, for instance, is given by

$$E_\alpha = \frac{\sum_n g_n E_n}{\sum_n g_n}, \quad (2)$$

where the sum on n extends over each atom within r_{cut}.

The coarse graining map is entirely determined by the choice of the parameter c, which sets the width of g_n and hence determines the spatial extent of the MD data influencing the value of the continuum field at α, which was found to be well converged when $r_{\text{cut}} \geqslant 3c$. A similar consideration of convergence found the maximum spacing between continuum points to be $d = 0.25c$.

The application of this coarse graining procedure to the potential energies of the pre-sheared glass is relatively straightforward. However, during the shear simulation it is necessary to compute such coarse-grained field quantities at a given time step. A proper continuum-level description requires a choice of either a Lagrangian or Eulerian frame. We have chosen a Lagrangian approach in what follows, as this is the typical description for solids. In the Lagrangian description, the material points are defined with respect to a reference configuration and continuum fields are functions of the reference coordinates $\mathbf{X}$ and current time t. In the case of the coarse-grained potential energy $E_\alpha = E_\alpha(\mathbf{X},t)$. Therefore, the MD system is only coarse-grained based on atomic positions in the initial configuration at $t = 0$ (before shear) and the evolution of E_α is determined by the changes in the potential energies of the atoms initially within the region surrounding α defined by r_{cut}.

The local atomic strain can also be calculated in a way that is consistent with this coarse graining method through an adaptation of a well-established definition of nonaffine displacement [15]. The measure of nonaffinity is determined by minimizing the mean-square difference between the actual displacements of the neighboring atoms relative to the central one and the relative displacements that they would have if they were in a region of homogeneous deformation. The square of the error D^2_{min} can be written as

$$D^2_{\text{min}} = \sum_n g_n^2 \sum_i \left(x_n^i - x_0^i - \sum_j F_{ij}\left(X_n^j - X_0^j\right)\right)^2. \quad (3)$$

The indices i and j denote Cartesian coordinates x^i at time t describing the spatial position of an atom during the shear and X^j in the reference configuration. The index n runs over the atoms within the coarse graining region surrounding α, where $n = 0$ is the reference atom with coordinates x_0^i and X_0^j, chosen to be closest to the centroid of the region. We have found that this choice for the reference atom is better than simply an arbitrary atom, which can present computational anomalies for regions with a small number of atoms or for large strains. Equation (3) differs from the original [15] in that it is a *weighted* least-squares formulation, and because it is generalized for finite deformations. The minimization of D^2_{min} allows a fit of the deformation gradient tensor F_{ij} from which the Green-Lagrange strain can be calculated as

$$\epsilon_{ij}^\alpha = \frac{1}{2}\left(\sum_k F_{ki}^\alpha F_{kj}^\alpha - \delta_{ij}\right). \quad (4)$$

In the following sections, the CuZr system studied using NEMD simulations has been coarse-grained according to the proposed methodology for selected length scales defined by $c = 5,16,32$, and 50 Å, where $c = 5$ Å and $c = 50$ Å correspond to the coarse-grained representations that are the finest and coarsest, respectively.

III. SIGNAL AND NOISE IN MOLECULAR DYNAMICS

The coarse graining methodology of the previous section efficiently reduces the vast number of DOF in the MD system by appropriately weighting the contributions of each atom within a given region surrounding a continuum point α and ensuring that the resulting coarse-grained representation of the field values at α are converged. The methodology relies entirely on the choice of the width of the Gaussian filter c and is amenable to local calculations of field quantities for each α, in particular the atomic strain, which requires knowledge of atomic positions in both reference and current configurations. In this section, we attempt to determine the range of values of c that best distinguishes regions inside the shear band from those outside it. Because spatial localization of both potential energy and atomic strain has been shown to characterize shear banding [53], we propose a criterion whereby the atomic strain computed at α, as described in the previous section, is used to analyze the evolution of the coarse-grained potential energies inside and outside the shear band. This enables us to study the effect of different coarse-grained representations on the identification of states inside and outside the band.

Herein, we define the shear band as simply the set of coarse-grained atomic strains that reach or exceed the net strain. More precisely the signal of the shear band is the set

$$\mathscr{S} = \left\{\epsilon_{12}^\alpha \middle| \epsilon_{12}^\alpha \geqslant \gamma\right\}, \quad (5)$$

where γ is the nominally imposed strain at the boundary [57]. Analogously, we define the background as the set of regions where the coarse-grained atomic strains are less than the nominally imposed strain at the boundary,

$$\mathscr{B} = \left\{\epsilon_{12}^\alpha \middle| \epsilon_{12}^\alpha < \gamma\right\}. \quad (6)$$

Figures 1–4 show the sets $\mathscr{S}$ and $\mathscr{B}$ as the system evolves from the purely elastic ramp-up, through the onset of the shear band, and into the flow-stress regime for the selected coarse graining length scales. It is important to note that we have only included the Cu atoms when applying Eq. (2) since the potential-energy distribution of each species is different. Either species however shows essentially the same results in terms of the onset of the shear band and the qualitative changes in the

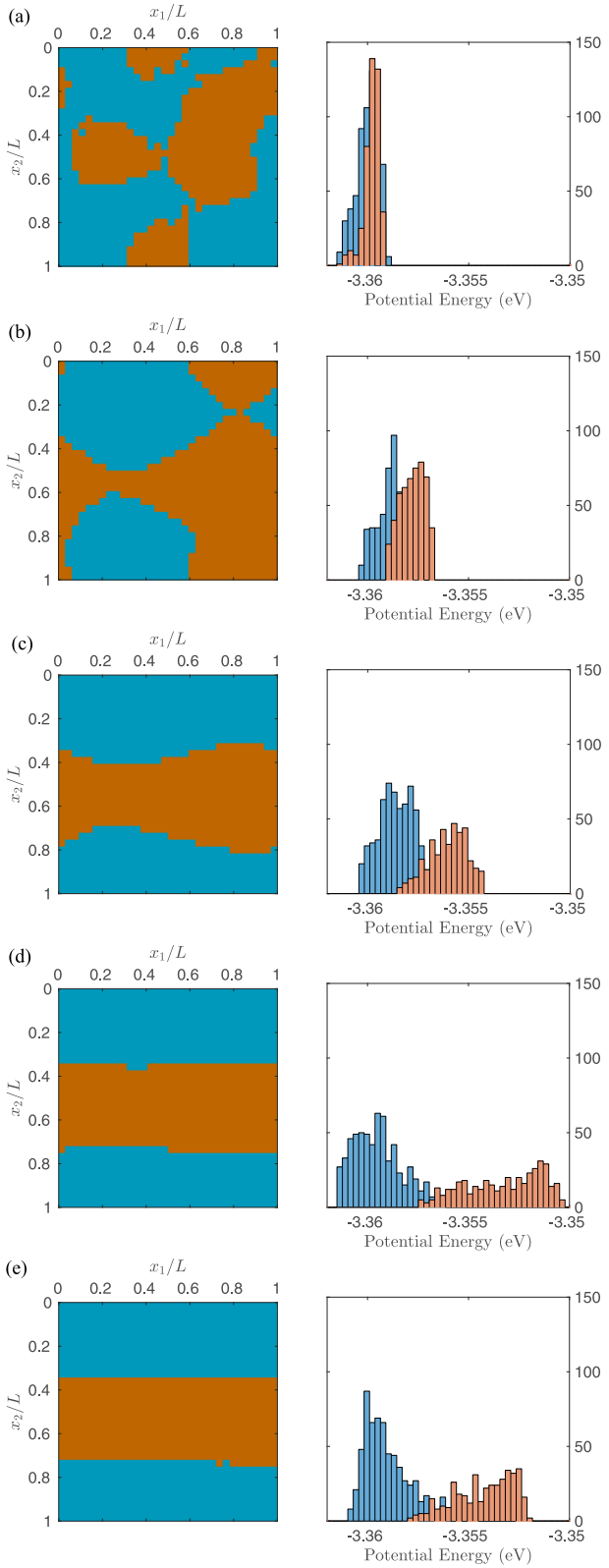

FIG. 1. Map (left column) of continuum points for a coarse-grained representation of the Cu atoms where $c = 50$ Å, defining the signal (orange) of the shear band and the background (blue). Histograms (right column) of the corresponding coarse-grained potential energies in the shear band and background. Configurations shown at a net strain of: (a) 3.5%, (b) 9.5%, (c) 10%, (d) 10.5%, and (e) 27.5%.

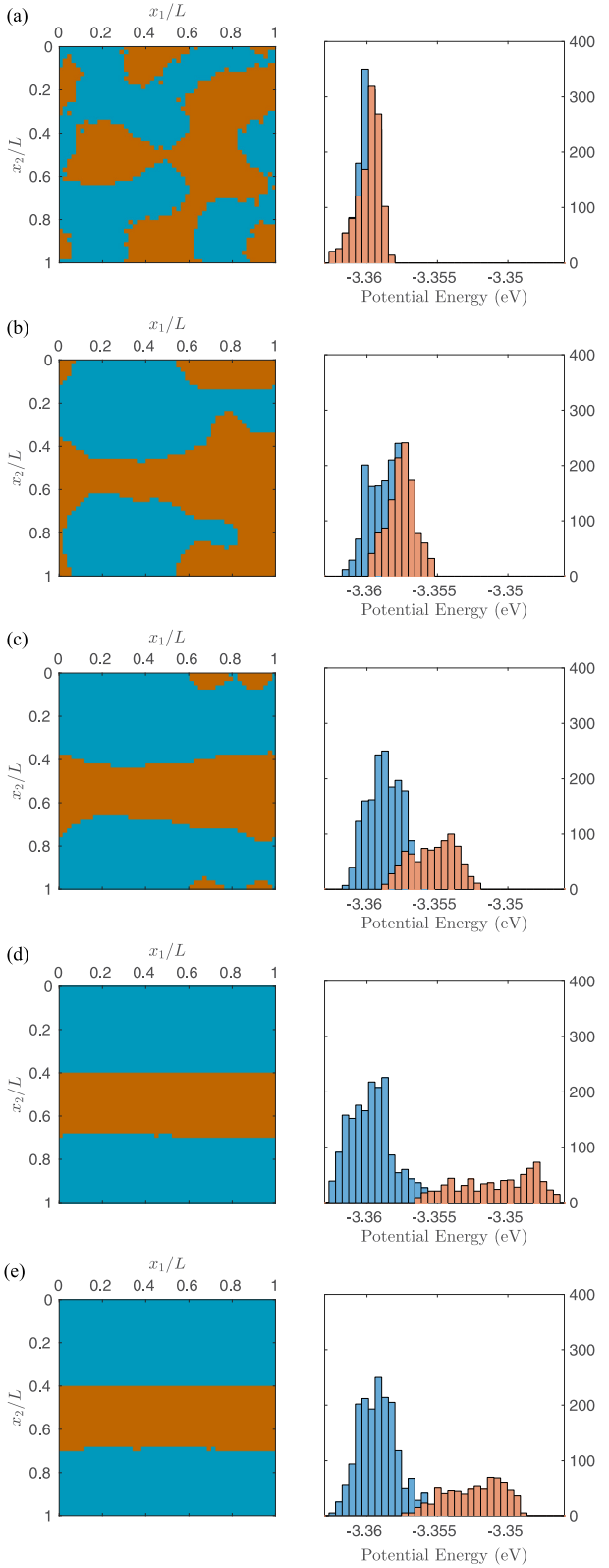

FIG. 2. Map (left column) of continuum points for a coarse-grained representation of the Cu atoms where $c = 32$ Å, defining the signal (orange) of the shear band and the background (blue). Histograms (right column) of the corresponding coarse-grained potential energies in the shear band and background. Configurations shown at a net strain of: (a) 3.5%, (b) 9.5%, (c) 10%, (d) 10.5%, and (e) 27.5%.

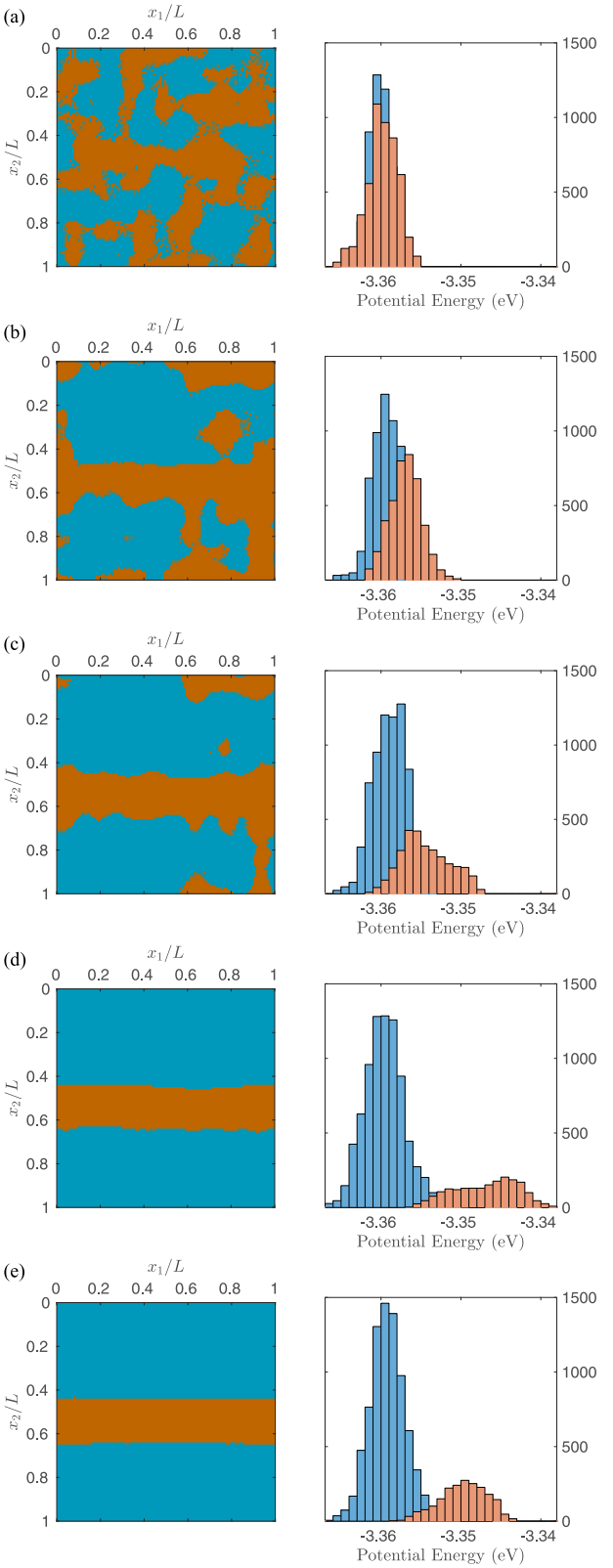

FIG. 3. Map (left column) of continuum points for a coarse-grained representation of the Cu atoms where $c = 16$ Å, defining the signal (orange) of the shear band and the background (blue). Histograms (right column) of the corresponding coarse-grained potential energies in the shear band and background. Configurations shown at a net strain of: (a) 3.5%, (b) 9.5%, (c) 10%, (d) 10.5%, and (e) 27.5%.

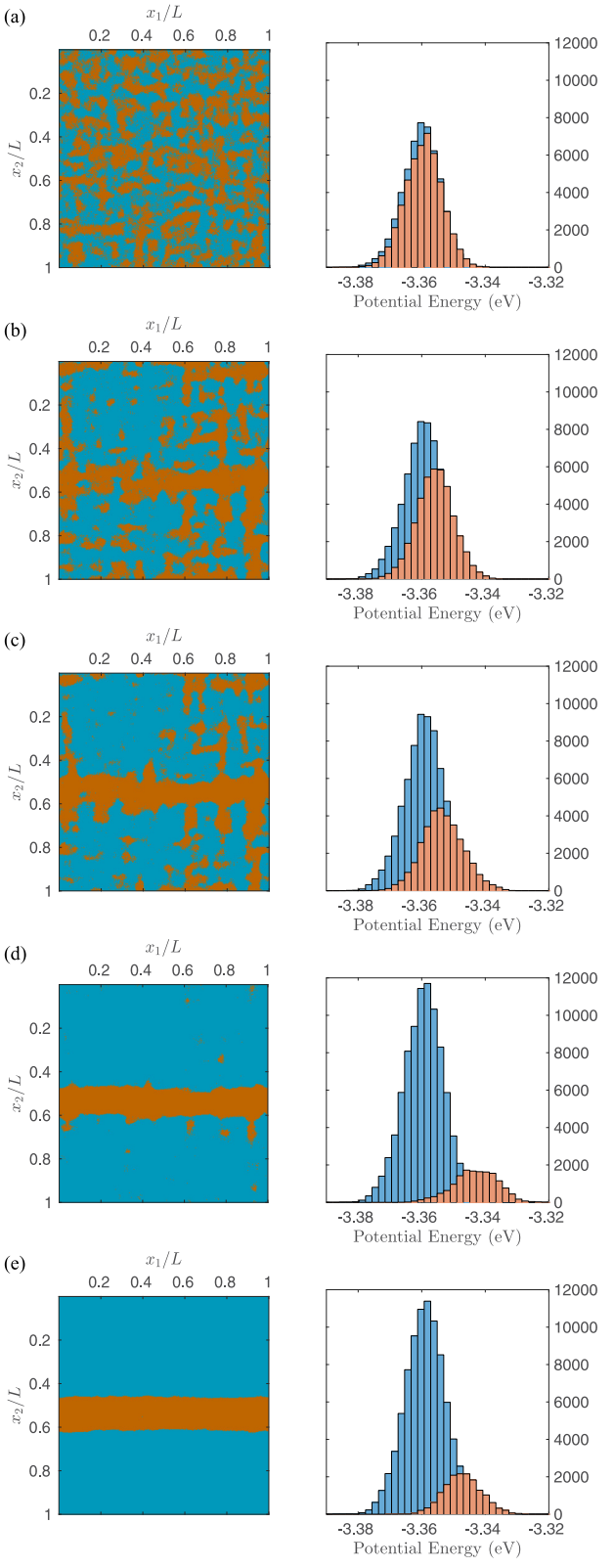

FIG. 4. Map (left column) of continuum points for a coarse-grained representation of the Cu atoms where $c = 5$ Å, defining the signal (orange) of the shear band and the background (blue). Histograms (right column) of the corresponding coarse-grained potential energies in the shear band and background. Configurations shown at a net strain of (a) 3.5%, (b) 9.5%, (c) 10%, (d) 10.5%, and (e) 27.5%.

TABLE I. The statistics of the coarse-grained potential energies in the signal and background distributions at different strains for a coarse-grained representation where $c = 50$ Å. The mean μ_s and standard deviation σ_s of the signal and the μ_b and σ_b of the background. The signal-to-noise ratio $\mathrm{SNR} = \frac{|\mu_s - \mu_b|}{\sigma_b}$ defines the strength of the shear band in the energy background.

Strain	μ_s	μ_{bg}	σ_s	σ_{bg}	SNR
3.5%	−3.3598	−3.3600	0.0004	0.0005	0.4377
9.5%	−3.3578	−3.3588	0.0006	0.0007	1.4735
10%	−3.3561	−3.3586	0.0009	0.0008	2.9933
10.5%	−3.3533	−3.3595	0.0019	0.0012	5.0282
27.5%	−3.3542	−3.3591	0.0014	0.0011	4.4564

distributions reflected in Figs. 1–4. The effect of considering only one of the species is further discussed in Sec. IV.

The signal and background plots in Figs. 1–4 feature an entirely mechanical response, in the sense that the distinction between signal states and background states is a binary choice based solely upon whether a given continuum point α has a local strain that satisfies the criterion of Eq. (5). However, this criterion for the mechanical response of the system can be directly related to the potential energy. The right side of Figs. 1–4 shows histograms of the potential energies corresponding to each α in $\mathscr{S}$ and $\mathscr{B}$, identifying the signal and background as two distinct potential-energy distributions. Using these energy distributions we define a signal-to-noise ratio (SNR) as

$$\mathrm{SNR} = \frac{|\mu_s - \mu_b|}{\sigma_b}, \tag{7}$$

where μ_s and μ_b are the means of the signal and background, respectively, and σ_b is the standard deviation of the background.

The emergence of the shear band can be readily seen through the relative changes in these distributions. In the purely elastic startup, the system exhibits a fluctuating mixture of signal and background without any strain localization. The average of $2\epsilon_{12}^{\alpha} = \gamma$ at all times during the deformation to satisfy compatibility. During the purely elastic regime, the signal and background possess nearly identical potential-energy distributions. The statistics of these two distributions are summarized in Table I as the system evolves for the representation where $c = 50$ Å. At 3.5% strain (still within the elastic regime) the means of the signal and background are nearly identical, and the SNR is very small.

The values of the SNR are shown in Fig. 5 as a function of the net strain for the different coarse-grained representations. A protoshear band begins to develop at 9.5% strain, and the two distributions begin to show a noticeable separation in their mean values. Figure 5 shows that while the shear band begins its initial stages of formation just prior to 9.5% strain, the signal $\mu_s - \mu_b$ appears to begin to significantly separate from the noise σ_b (when $\mathrm{SNR} > 1$) for $c = 50$, 32, and 16 Å. This indicates that the SNR after banding is improved by considering larger coarse-grained representations, but that the onset of the shear band itself is detected equivalently as long as this coarse graining exceeds $c = 16$ Å.

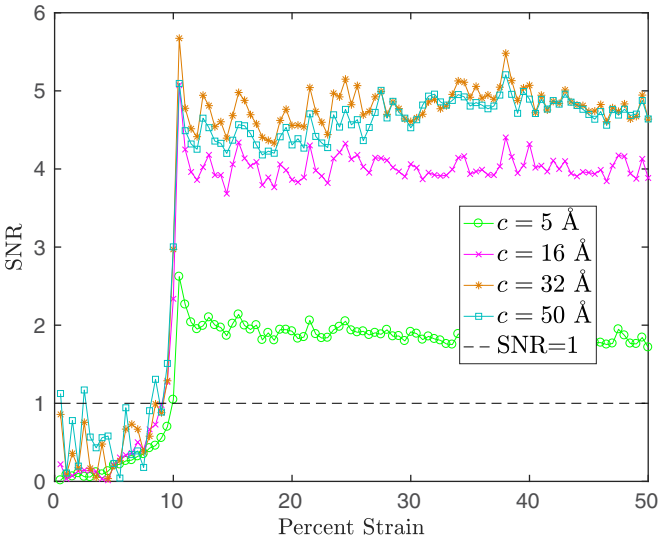

FIG. 5. The SNR as function of global strain for different coarse-grained representations defined by c in g_n. The signal $\mu_s - \mu_b$ exceeds the noise σ_b only when $\mathrm{SNR} > 1$ (dashed line).

The shear band is fully formed across the system at 10.5% strain, as can be seen at each level of coarse graining shown in Figs. 1–4. This also corresponds to the largest SNR value, evidenced by both the most significant separation in the means of the distributions as well as the occupation of the highest energy states. Once the signal and background distributions have distinctly separated, they remain so throughout the shear simulation. We have observed that once the shear band has formed at approximately 10.5% strain, the SNR tends to monotonically increase with the width of the coarse graining, until saturating for $c \geqslant 32$ Å as Fig. 5 shows. We note that the minimum-image convention places a limit on the size of any coarse graining region surrounding a given α relative to the size of the simulation cell, namely we must ensure $r_{\mathrm{cut}} \leqslant L/2$.

IV. EFFECTIVE-TEMPERATURE MODEL

The coarse graining methodology and corresponding analyses presented thus far suggest that coarser-grained representations may better capture the shear banding seen when the methodology is applied to NEMD shear simulations of a CuZr glass. To further evaluate the suitability of the different coarse graining length scales and their affect on the ability to predict the system's mechanical response, we now turn to the preparation of the initial condition of the STZ theory.

One critical feature of the STZ theory is its ability to describe the structure of an amorphous solid through a continuum scalar field of *effective temperature* [30–38] T_{eff} that is defined as

$$T_{\mathrm{eff}} = \frac{\partial U_c}{\partial S_c}, \tag{8}$$

where U_c and S_c are the amorphous system's potential energy and entropy, respectively, of only the configurational DOF, i.e., those DOF describing the structure of the material [5–7,35–37] and operating on timescales no shorter than those associated with molecular rearrangements. This is to be

distinguished from the more familiar, thermalized temperature T, which accounts for the fast, kinetic DOF, which relax on time scales short compared to the timescales associated with plasticity. The typical definition of T is applicable to the vibrational DOF, which remain in thermodynamic equilibrium. The configurational DOF constitute an enumerable set of specific potential-energy configurations of the atoms, which correspond to low-lying minima in the potential-energy landscape of the amorphous solid. They are often referred to as the system's "inherent structures" [6]. An STZ rearrangement that occurs during plastic deformation corresponds to the state of the system transitioning from one inherent structure (local minimum) to a neighboring one. In the effective-temperature STZ formalism, a dimensionless scalar field $\chi = \chi(\mathbf{X},t)$ is defined as

$$\chi \equiv \frac{k_B T_{\text{eff}}}{E_z}, \tag{9}$$

where k_B is the Boltzmann factor and E_z is the STZ formation energy. Although χ is a dimensionless form of T_{eff} we shall henceforth refer to it as simply "the effective temperature" for readability. Some limited attempts to experimentally measure an effective temperature for disordered materials have been made [58], as well as other direct, quantitative comparisons with experiments of bulk metallic glasses [59].

For a monotonically loaded, athermal amorphous system where there are no rate-dependent processes such as aging, which compete with the STZ-transition rates described in Sec. I, and where we assume there to be a low STZ density, the flow rule for the plastic component of the rate-of-deformation tensor $\mathbf{D}^{\text{pl}}$ follows from the STZ theory with the form,

$$\mathbf{D}^{\text{pl}} = \begin{cases} \mathbf{0}, & ||\tilde{\mathbf{S}}|| < 1 \\ \frac{\epsilon_0}{\tau_0} e^{-1/\chi}\left(1 - \frac{1}{||\tilde{\mathbf{S}}||}\right)\mathbf{F}, & ||\tilde{\mathbf{S}}|| \geqslant 1, \end{cases} \tag{10}$$

where $\mathbf{F} = \mathbf{F}(\tilde{\mathbf{S}})$ is a monotonic tensor-function of the deviatoric Cauchy stress $\tilde{\mathbf{S}}$, which is normalized in terms of the yield stress s_y. When $||\tilde{\mathbf{S}}|| < 1$ there are no plastic rearrangements and $\mathbf{D}^{\text{pl}} = 0$. A family of symmetric functions of the stress has been identified as having the correct properties for $\mathbf{F}$, such as $\mathbf{F} \to 0$ when $\tilde{\mathbf{S}} \to 0$ and $\mathbf{F}$ grows linearly as $\tilde{\mathbf{S}} \to \infty$ [60,61]. For simplicity we have chosen the form

$$\mathbf{F} = -2 + ||\tilde{\mathbf{S}}|| + \exp(-||\tilde{\mathbf{S}}||)(2 + ||\tilde{\mathbf{S}}||), \tag{11}$$

which has been shown to be effective in one-dimensional continuum STZ analyses [62]. The parameter $1/\tau_0$ is the inherent attempt frequency of the material, which is close to the Einstein frequency, and sets a timescale for the "flips" or rearrangments of the STZs. The average STZ contains an approximate number of atoms denoted by the value of ϵ_0.

In the athermal limit the dynamical equation for the effective temperature χ takes the form

$$c_0 \dot{\chi} = \tilde{\mathbf{S}} : \mathbf{D}^{\text{pl}}(\chi_\infty - \chi) + \nabla \cdot D_\chi \nabla \chi \ . \tag{12}$$

The first term on the right-hand side in Eq. (12) represents the plastic work per unit time done on the configurational DOF when $||\tilde{\mathbf{S}}|| > 1$. The parameter c_0 is a specific-heat-like quantity that relates the heat flowing into the configurational DOF to the resulting increase in the effective temperature. In flowing regions χ converges to a limiting value χ_∞, which represents the steady-state effective temperature where the work done to shear the amorphous material no longer causes an increase in disorder. The final term in Eq. (12) describes the diffusion of the effective temperature through a rate-dependent diffusivity $D_\chi = l^2\sqrt{\frac{1}{2}\mathbf{D}^{\text{pl}} : \mathbf{D}^{\text{pl}}}$ with dimensions length-squared per unit time, where the length scale l is approximately the size of an STZ (on the order of a molecular length scale). Because D_χ is a function of the plastic rate-of-deformation, the diffusivity is inhomogeneous and the effective temperature diffuses at different rates in different regions of the material. For example, in regions where the local plastic-strain rate is larger, so too is the value of D_χ.

The initial value of the effective-temperature field $\chi_0 = \chi_0(\mathbf{X})$ characterizes the structure of the glass in the presheared state, and ideally would come from an analysis of the atomistic information of the system's constituents. In the absence of this per-atom information, the form of χ_0 including the mean value and fluctuations about the mean are usually chosen in a way to best match the macroscopic behavior, e.g., the stress-strain curves of the material. The ability of the fluctuations in χ_0 to grow and lead to strain localization in the form of a shear band depends on both the mean value of χ_0 and the amplitude of the fluctuations [62,63], which underscores the need for χ_0 to capture the structural state of the pre-sheared glass with the appropriate level of physical detail.

Previous STZ-theory approaches that have attempted to model the NEMD shear deformation of Lennard-Jones glasses have relied upon postulating a value for χ_0 *a priori* without directly extracting it from actual atomistic data, such as the potential energies [59,62,64,65]. These STZ-effective-temperature simulations were also entirely one-dimensional, but nonetheless have provided important guidance for the development of more sophisticated techniques. Although it is important to note that the range of acceptable values of χ_0 for a particular system is significantly restricted by the nonlinear form of Eq. (12) and its stability.

A determination of χ_0 from the presheared glass would in principle come from a direct calculation of the derivative in Eq. (8). This could be achieved by enumerating the set of inherent structures and considering their density-of-states, thus determining the corresponding S_c and T_{eff} at a given U_c. At the moment however, such a calculation remains computationally intractable. Moreover, in practice temperatures are usually determined from equations of state or through a heat capacity, and the necessity of directly measuring entropic changes is therefore avoided. In devising a simpler procedure here to relate effective temperature to atomic potential energy, we follow a similar approach. We note that there is already evidence suggesting the average atomic potential energy of a simple Lennard-Jones system [53] is linearly related to χ.

In the context of the coarse-grained potential energies coming from Eq. (2), an assumption of linearity allows us to compute an effective temperature at a given α as

$$\chi_\alpha^{\text{MD}} = \beta \frac{\sum_n g_n(E_n - E^o - E^{\text{el}})}{\sum_n g_n}, \tag{13}$$

where the parameter β is a material specific constant with units of inverse potential energy per atom and can be related to a specific heat [53]. The reference energy E^o corresponds to a

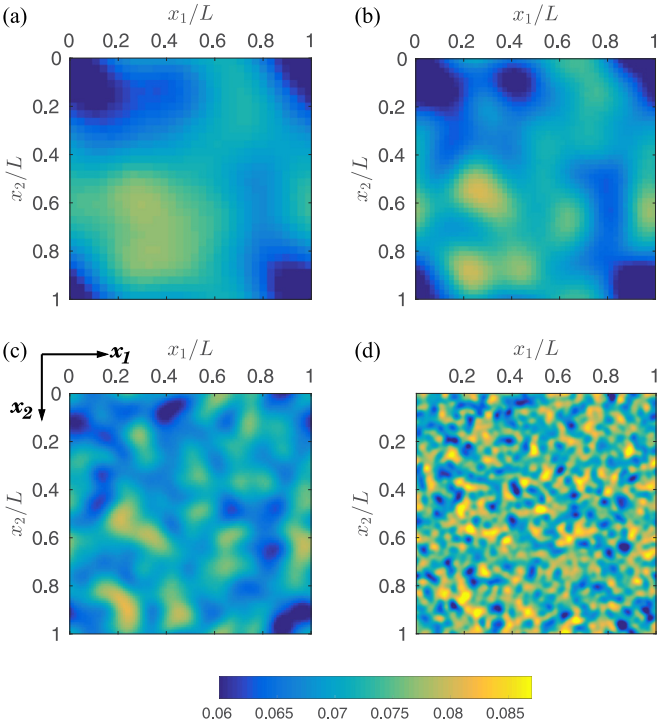

FIG. 6. The initial condition of the effective temperature in the STZ theory χ_0 using different coarse-grained representations: (a) $c = 50$ Å, (b) $c = 32$ Å, (c) $c = 16$ Å, and (d) $c = 5$ Å.

state of no disorder in the glass, where by definition $T_{\text{eff}} = 0$. Equation (13) introduces E^o and β as yet unknown parameters, but now with the advantage of being able to directly relate averages of atomic potential energy per atom to χ. We have further shifted E_n by removing the effect of the linear-elastic strain energy, since changes in χ occur only in the presence of a nonzero plastic-strain rate. Linear-elastic strain energy is given by $\mathscr{W} = \frac{1}{2} C_{ijkl}\epsilon_{ij}\epsilon_{kl}$, where C_{ijkl} is the Hookean-elasticity tensor, and therefore the per-atom elastic-strain energy E^{el} is found by a fit to the parabolic portion of the system's total potential-energy density as a function of shear strain ϵ_{12}. This is an approximation that becomes an exact correction in the limit where all elastic behavior is perfectly linear.

Figure 6 shows the result of applying Eq. (13) and the values of Table III to the as-quenched configuration of the glass, yielding coarse-grained representations of the system before shear $\chi_\alpha^{\text{MD}}(\gamma = 0)$ for different c. These images of the initial conditions reveal how the levels of coarse graining affect the spatial variation of χ. The coarser representations tend towards a smoother, more localized field. For instance, when $c = 50$ Å and $c = 32$ Å, the highest values of χ_0 reside in the bottom left quadrant of the grid, and are likely sites for the growth of a particular instability that can lead to strain localization.

The same procedure described by Eq. (13) is applied to determine χ_α^{MD} for subsequent configurations as the system is subjected to a state of simple shear. The left column of Figs. 7–10 shows the evolution of χ_α^{MD} at different increments of the system's net strain during the NEMD shear simulation. The

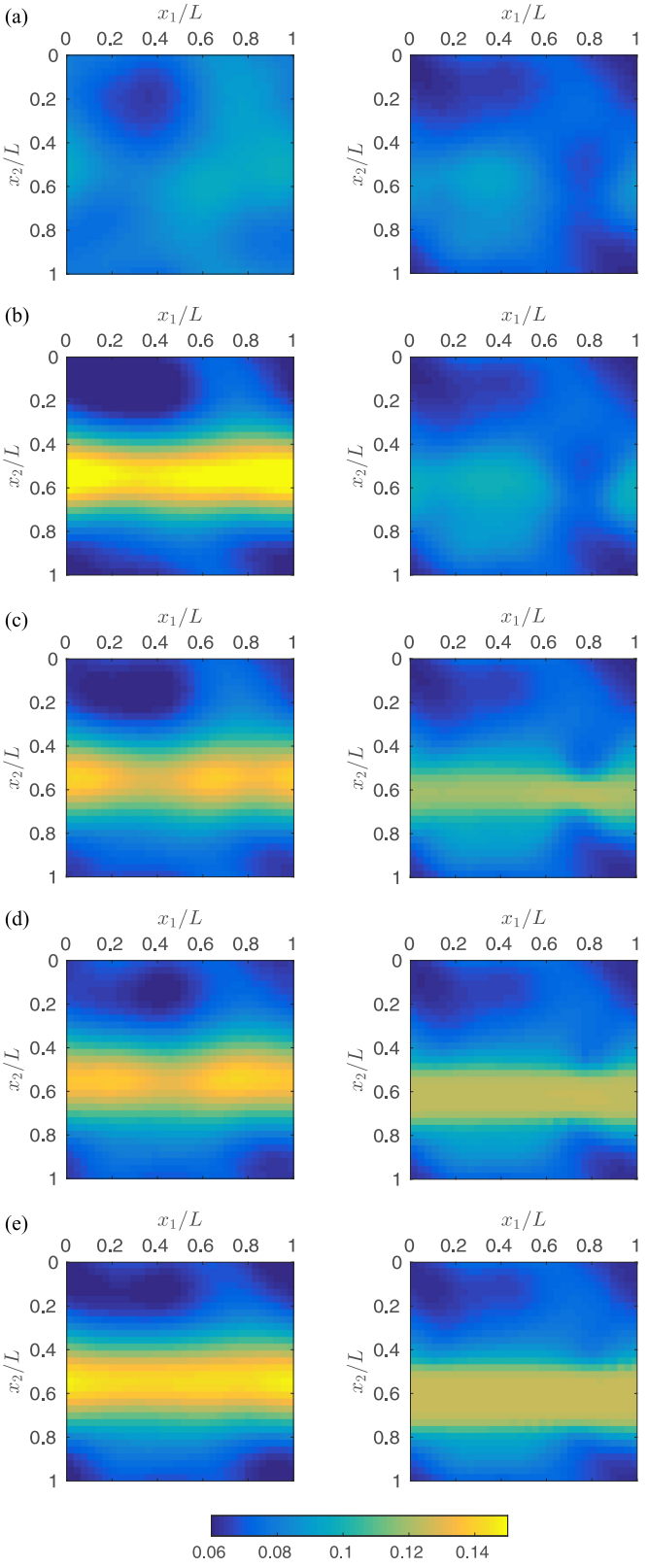

FIG. 7. The coarse-grained effective temperature of the NEMD shear simulation (left column) χ_α^{MD} and the effective temperature of the STZ theory (right column) χ, where the system is coarse-grained using $c = 50$ Å at: (a) 9.5%, (b) 10.5%, (c) 15.5%, (d) 27.5%, and (e) 42% net strain.

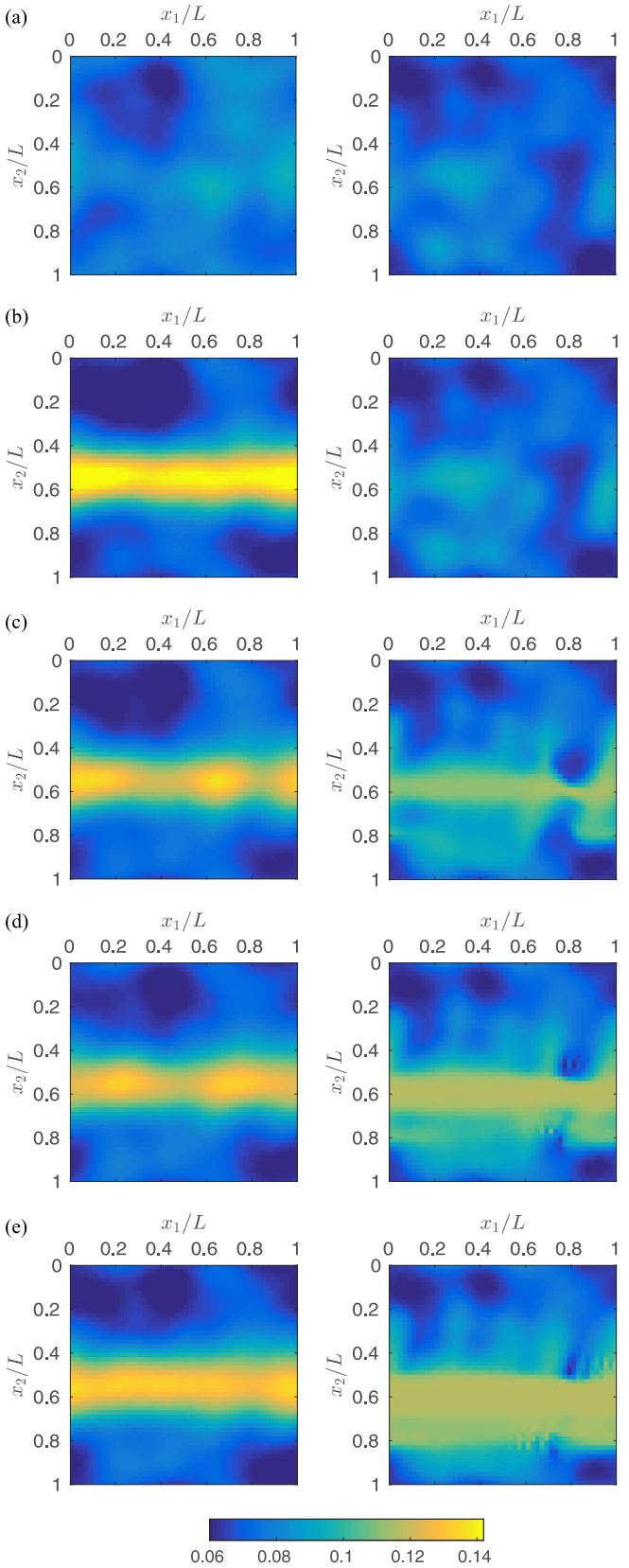

FIG. 8. The coarse-grained effective temperature of the NEMD shear simulation (left column) $\chi_\alpha^{\mathrm{MD}}$ and the effective temperature of the STZ theory (right column) χ where the system is coarse-grained using $c = 32$ Å at: (a) 5%, (b) 9.5%, (c) 10.5%, (d) 15.5%, (e) 27.5%, (f) 42%, and (g) 49.5% net strain.

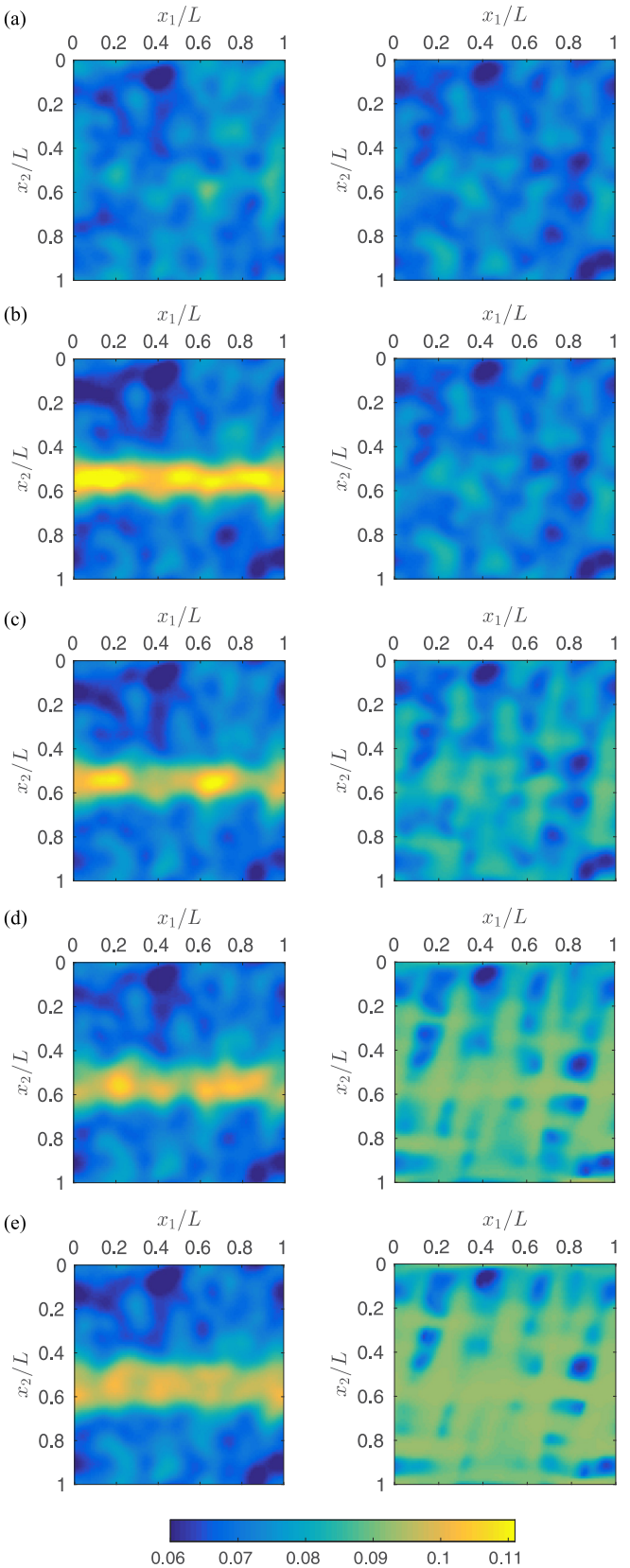

FIG. 9. The coarse-grained effective temperature of the NEMD shear simulation (left column) $\chi_\alpha^{\mathrm{MD}}$ and the effective temperature of the STZ theory (right column) χ where the system is coarse-grained using $c = 16$ Å at: (a) 5%, (b) 9.5%, (c) 10.5%, (d) 15.5%, (e) 27.5%, (f) 42%, and (g) 49.5% net strain.

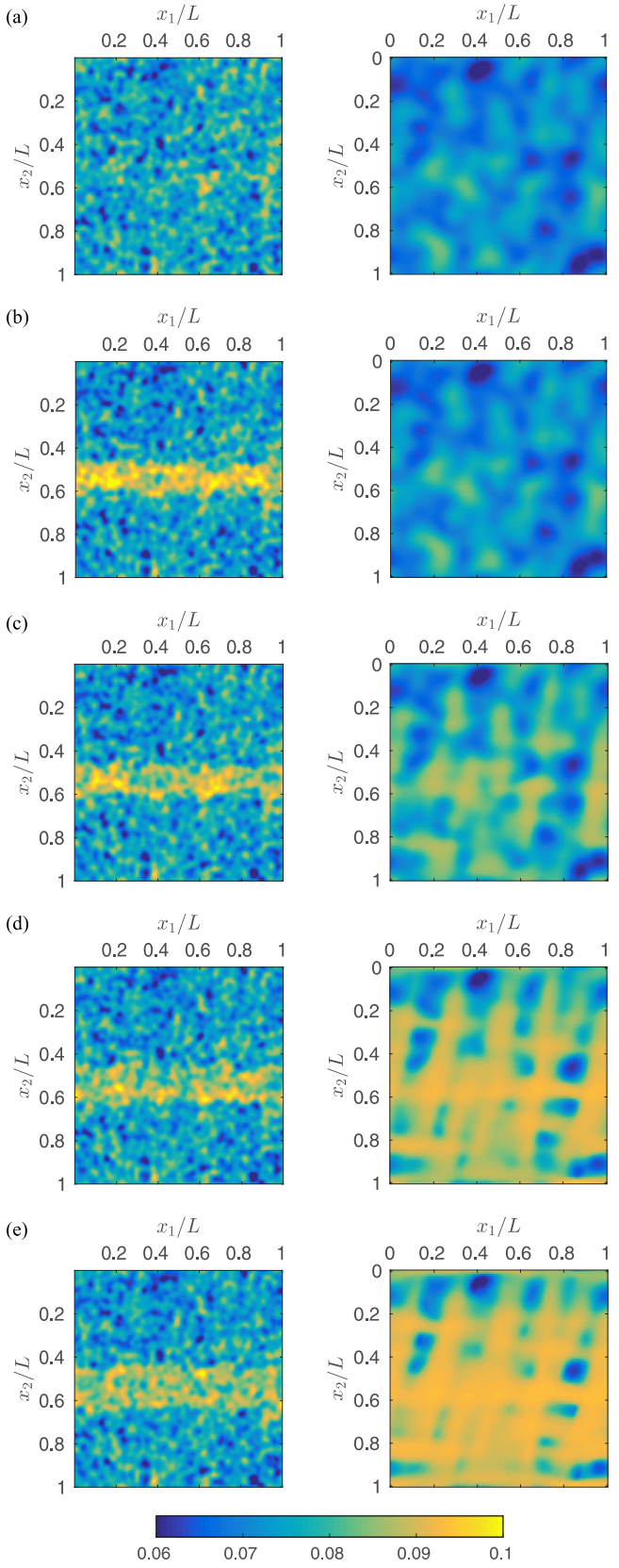

FIG. 10. The coarse-grained effective temperature of the NEMD shear simulation (left column) $\chi_\alpha^{\mathrm{MD}}$ and the effective temperature of the STZ theory (right column) χ, where the system is coarse-grained using $c = 5$ Å at: (a) 5%, (b) 9.5%, (c) 10.5%, (d) 15.5%, (e) 27.5%, (f) 42%, and (g) 49.5% net strain.

formation of the shear band here proceeds in a manner similar to that depicted in Figs. 1–4, which show the evolution of signal and noise states under the strain criterion. As mentioned in Sec. III we have arbitrarily chosen only one of the species, the Cu atoms, to include in the sum in Eq. (13). We have found, however, that choosing either species gives very similar results for a particular g_n, including the signature of the shear band. This would confirm that both species contain similar, relevant structural information. We note, however, that while only one species is explicitly considered, the Cu-Zr-interactions are still present through the potential energies of the atoms of either species.

Recently a numerical method for simulating the deformation of elastoplastic materials in the quasistatic limit has been developed [66] by building on a mathematical correspondence with the incompressible Navier-Stokes equations. It is well-suited for a large class of materials, which typically undergo small elastic deformations and feature large elastic wave speeds, making many plastic deformation problems intrinsically quasi-static. In such situations, this method allows simulating realistic loading rates, which would be prohibitively computationally expensive using explicit methods [67].

Here we use the methodology of Sec. II to provide an initial condition for the effective-temperature field and then simulate the continuum STZ model using the two-dimensional quasistatic numerical implementation. The quasistatic condition requires

$$\nabla \cdot \boldsymbol{\sigma} = \mathbf{0}\,. \tag{14}$$

and is equivalent to the inertial limit where $\boldsymbol{\sigma}$ is the Cauchy stress tensor. This numerical approach is most suitable for materials that can be well-described by the additive decomposition of the rate-of-deformation tensor into elastic and plastic parts, namely

$$\mathbf{D} = \mathbf{D}^{\mathrm{el}} + \mathbf{D}^{\mathrm{pl}}, \tag{15}$$

and is generally a good assumption when elastic strains are small. The model can be solved by connecting the flow rule for the plastic-strain rate to Newton's laws for deformable bodies by

$$\frac{\mathcal{D}\boldsymbol{\sigma}}{\mathcal{D}t} = \mathbf{C} : \mathbf{D}^{\mathrm{el}} = \mathbf{C} : (\mathbf{D} - \mathbf{D}^{\mathrm{pl}}), \tag{16}$$

where $\mathbf{C}$ is the Hookean-elasticity tensor and $\frac{\mathcal{D}}{\mathcal{D}t}$ refers to the Jaumann objective rate. To simulate the simple shear deformation of the NEMD results in Sec. II the velocity $\mathbf{v}(\mathbf{x},t)$ is fixed at the top and bottom of the system in the direction of shear by the imposed shear-strain rate,

$$\mathbf{v}(x_1,0,t) = \dot{\gamma} L \mathbf{e}_1 \qquad \mathbf{v}(x_1,L,t) = \mathbf{0}, \tag{17}$$

while

$$\frac{\partial \boldsymbol{\sigma}}{\partial x_2} = \frac{\partial \chi}{\partial x_2} = 0 \tag{18}$$

at $x_2 = 0$ and $x_2 = L$. These boundary conditions and the model's numerical implementation developed in Ref. [66] describe a system that is periodic in the direction of shear (x_1) but not in the perpendicular direction. This is unlike the simulation box in the NEMD simulations which is periodic in all directions. While these differences in boundary conditions

TABLE II. The parameters of the STZ effective-temperature model used in all coarse-grained representations. The "−" indicates the parameter is dimensionless.

PARAMETERS		UNIT	Value
Yield stress	s_y	GPa	0.85
STZ size	ϵ_0	—	10
Inverse attempt frequency	τ_0	ps	0.1
Elastic shear modulus	μ	GPa	20
Plastic-work fraction	c_o	—	0.3
Global shear rate	$\dot{\gamma}$	ps^{-1}	10^{-4}
Diffusivity length	l	Å	4.01

could possibly affect the continuum model's ability to predict shear band formation at the top or bottom boundaries, in all the simulations reported here the shear band forms near the center of the system.

The values of the parameters of the effective-temperature model are summarized in Table II, which are the same across simulations of different coarse-grained initial conditions. The value of the elastic shear modulus μ in the STZ theory was set to match the linear-elastic regime of the atomistic simulation where $c = 50$ Å, in particular the linear-elastic portion of the stress-strain curve shown in Fig. 11. Values for ϵ_0 and s_y were taken from previous investigations of metallic glasses [67]. The fraction of plastic work c_0 was chosen to best match the shape of the stress-strain curve of the atomistic simulation where $c = 50$ Å. Previous studies involving far simpler, one-dimensional analyses have indicated that c_0 should be on the order of unity [62], and earlier STZ-theory simulations have reported values between 0 and 1 [66,67]. Here we initially performed the STZ-theory simulations using $c_0 = 1$ and then adjusted c_0 to match the stress overshoot and the softening behavior of the atomistic simulations. Changes in c_0 adjust how slowly or quickly χ reaches χ_∞ and consequently affect the shape of the stress-strain curve as well as the evolution of χ itself. The length scale contained in the prefactor of the

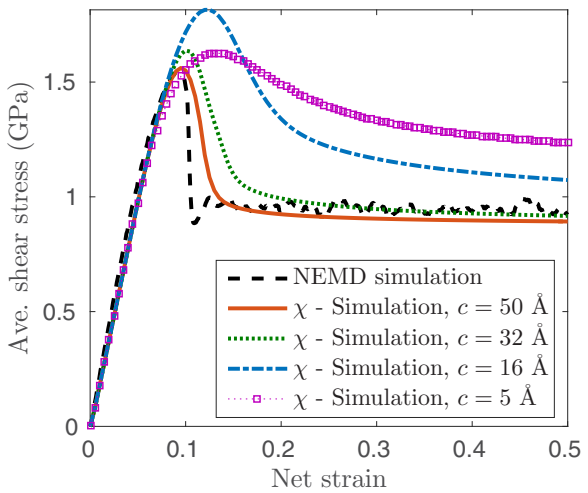

FIG. 11. The average shear stress S_{12} of the CuZr MD simulation (dashed curve) and continuum effective-temperature theory (solid curves) for different coarse-grained initial conditions χ_0.

TABLE III. The values of β and E^o in the potential-energy mapping to effective temperature given by Eq. (13) and the steady-state effective temperature χ_∞ for different coarse-grained representations defined by c.

c (Å)	β	E^o (eV)	χ_∞
50	9.5	−3.367	0.13
32	6.1	−3.371	0.12
16	2.3	−3.390	0.094
5	0.92	−3.440	0.085

diffusivity, in general, is strictly constrained by the choice of the time step used during the STZ-theory simulation. Here, we initially attempted values of l that were on the order of the size of the developing shear banding, since l is also related to the length of the interfacial region between the shear band and the material outside the band. The value of l in Table II enabled the best agreement between the evolution of χ and $\chi_\alpha^{\mathrm{MD}}$ when $c = 50$ Å by allowing the shear band to broaden (in the x_2 direction) as much as possible while inhibiting the tendency for regions outside the band to disorder, a phenomenon not observed in the molecular dynamics simulations.

The values in the mapping described by Eq. (13), β and E^o, were chosen so that the initial condition $\chi_0 = \chi_\alpha^{\mathrm{MD}}(\gamma = 0)$ effected the best agreement between the NEMD simulation and STZ theory and vary slightly as a function of c as summarized by Table III. Unlike the values of the STZ parameters, which are the same for all the STZ-theory simulations regardless of the level of coarse graining, β and E^o must be chosen separately for each value of c. The choice of β and E^o was found to have the most dramatic effect on the behavior of the model. While the STZ parameters essentially control the rates of the evolution of the amorphous system, the values of β and E^o determine the initial condition and hence whether it is even possible for shear banding to occur. Initially, β and E^o were chosen so that the mean of χ_0 for each level of coarse graining was within the range of the mean χ_0 reported in previous work [62] and then adjusted to best match the atomistic simulation with respect to both the stress-strain curve and the evolution of $\chi_\alpha^{\mathrm{MD}}$. The steady-state condition for the effective temperature χ_∞ similarly depends on the level of coarse graining but is precisely calculable once β and E^o, and therefore Eq. (13), have been determined. The set $\mathscr{S}$ defined in the analysis of Sec. III can be used to identify the $\chi_\alpha^{\mathrm{MD}}$ inside the shear band, and the average of $\chi_\alpha^{\mathrm{MD}}$ in $\mathscr{S}$ at 50% net strain is then taken to be χ_∞. The average of this flowing region varied only slightly for different values of c as seen in Table III.

The right column of Figs. 7–10 shows the effective temperature of the STZ theory evolving as the system is sheared. Each figure illustrates the effect of a particular level of coarse graining that is applied to the same initial configuration of atomic potential energies. The same grid resolution determined by the convergence criteria discussed in Sec. II is used for both χ and $\chi_\alpha^{\mathrm{MD}}$. At 10.5% strain the shear band, which is readily apparent in $\chi_\alpha^{\mathrm{MD}}$ of the NEMD simulation, is somewhat delayed in χ of the continuum model. The increase in χ in the model near the center does indicate the formation of a shear band, but this is not continuous across the

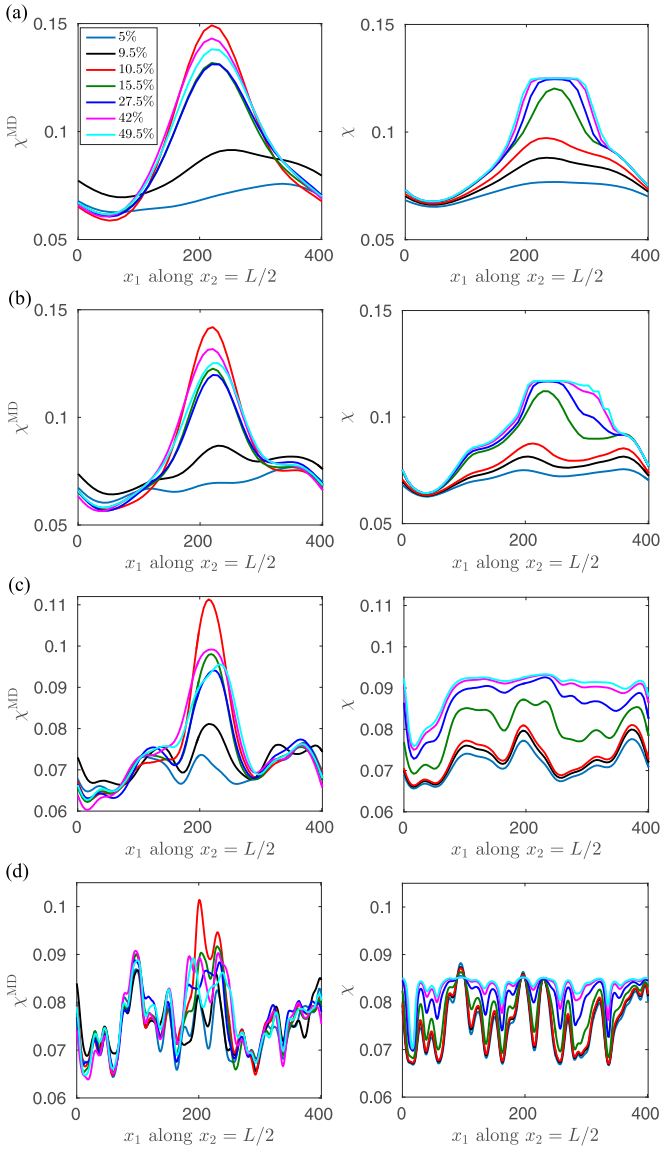

FIG. 12. The coarse-grained effective temperature of the NEMD shear simulation (left column) $\chi_\alpha^{\mathrm{MD}}$ and the effective temperature of the STZ theory (right column) χ along $x_1 = L/2$ where the system is coarse-grained for: (a) $c = 50$ Å, (b) $c = 32$ Å, (c) $c = 16$ Å, and (d) $c = 5$ Å.

system until about 11.5% strain, and takes slightly longer to reach χ_∞ in the center of the band. Figure 12 shows the value of $\chi_\alpha^{\mathrm{MD}}$ and χ along a one-dimensional slice at $x_1 = L/2$, and highlights the sharpest contrast among the different coarse-grained representations and their effect on the predictability of χ in the continuum description. Coarser representations, i.e., $c = 50$ Å and $c = 32$ Å certainly appear to better capture the size (width) and location of the shear band, while finer coarse-grained representations lead to a proliferation of noise that in turn leads to numerous individual shear bands and a subsequent system-wide, uniform disordering that is not reflected in the NEMD simulations. The effect of the initial condition is also apparent from the stress-strain curves in Fig. 11. The stress-strain histories further support the notion that the coarser representations provide a more accurate continuum picture. The stress-strain curves for $c = 50$ Å and $c = 32$ Å exhibit a strong stress-overshoot and subsequently a distinct softening period, which is indicative of the plastic strain being accommodated within some region of the system. This is in contrast to the curves for $c = 16$ Å and $c = 5$ Å, which reflect a less-ordered structure that undergoes the more uniform disordering also seen in the Fig. 12.

V. CONCLUSIONS

We have presented a study of shear banding using NEMD simulations and a two-dimensional numerical implementation of the continuum STZ effective-temperature theory. The coarse graining methodology used in this work has been developed with the phenomena-dependent focus of capturing the primary mode of deformation of metallic glasses, shear banding. The methodology is an attempt to identify and directly link the atomistic descriptors of the system, e.g., the local potential energy, to the initial condition for the effective-temperature in the STZ model to develop a well-informed, predictive continuum description of the plasticity. Such a description would permit rapid evaluation of material response for amorphous systems. It would further enable quantitative performance assessment through quantification of variability and uncertainty in material response in an efficient manner without the need for large-scale, computationally intensive atomistic simulations.

In the STZ theory the effective temperature is the continuum-based measure of the shear-induced disordering of a material's structure, and as per its definition with respect to the configurational energy and entropy of the system, should evolve closely with the material's potential energy. We have found that to be the case here, but also that the continuum model's accuracy is significantly dependent on how the atomic information is coarse-grained, which affects the properties of the resulting initial condition and the ability to make one-to-one comparisons between the coarse-grained NEMD and the effective temperature theory. Our analysis indicates that coarser-grained representations between $c = 32$–50 Å appear to best resolve the variations from the average in atomic potential energy data so that an instability in χ_0 can grow, diffuse, and saturate in a way that corresponds accurately to the NEMD results. Indeed, the primary conclusion of this investigation is that there exists a coarse graining length scale at which the effective-temperature description in the STZ theory becomes capable of accurately describing the mechanical response and microstructural evolution. Below this length scale the concept of effective temperature appears to beak down and is no longer useful as a material property.

The steady-state effective temperature χ_∞, which enters the theory as a well-defined material-dependent property, also supports this conclusion. When $c = 32$–50 Å, χ_∞ appears to converge to a single value. In prior work [53], χ_∞ was approximated to be the effective temperature that corresponds to the glass transition temperature T_g, and from this assumption E_z was estimated directly from Eq. (9), namely $E_z = k_B T_g/\chi_\infty$. In the case of our work here, using a reported value of $T_g \approx 700$ K [68] when $c = 50$ Å and $\chi_\infty = 0.13$ results in $E_z \approx 0.45$ eV, which is very similar to the prior estimate reported in Ref. [53]. Most interesting, however, is that these

computed values of E_z from the STZ theory are within the same range as the activation barriers (0.32 eV) associated with shear band flow in recent experiments of Vitreloy [69]. This suggests STZ creation may be the rate-limiting step in mediating shear band flow.

Both the location and width of this flowing region in the effective-temperature model compare well with the corresponding changes in $\chi_\alpha^{\mathrm{MD}}$ when $c = 50$ Å and $c = 32$ Å. The difference in strain between the onset of a fully formed shear band that is continuous and visible across the MD system and that observed in the effective-temperature model is approximately 5–6% as seen in Figs. 7(c) and 7(d). The results of the STZ-effective-temperature modeling in this study are the only ones we know of in which model validation has been derived directly from atomistic simulation. Both the microstructural evolution and the stress-strain response have been directly compared with the results of the NEMD simulation, which itself employs a well-established EAM potential.

Despite a good deal of measurable agreement using the methodology presented here, this analysis is incomplete and has left us with a number of important questions. The optimal length scale for the coarse graining, i.e., what the value of c in g_n should be, is not completely clear. While the value of the SNR increases with c after the shear band forms, analysis of the SNR does not provide clear guidance by itself as to the selection of a unique optimal c, although it does indicate that there is a minimal value of c. A study of the range of the parameters β and E^o that are critical for determining the initial conditions from the coarse-grained atomistic data that lead to shear banding would be beneficial in guiding constitutive theory development, but also, eventually, in guiding alloy development. Criteria for the ability of a single perturbation off a flat, uniform χ_0 to grow and localize into a shear band in one-dimension have already been preformed [62]. More generalized criteria still need to be developed to apply to the two- and three-dimensional coarse-grained atomistic data under nonidealized conditions, e.g., where there exist fluctuations from the background with a nonzero mean. An understanding of this sort could connect the level of coarse graining directly to the initial condition, and allow acceptable levels of coarse graining that optimize shear banding to be more clearly defined.

ACKNOWLEDGMENTS

The authors kindly thank C. Robert E. Maaß and Mark O. Robbins for comments and suggestions during the course of this work. Support was provided by NSF Grant Awards No. DMR-1107838, No. DMR-1408685, and No. DMR-1409560. A.R.H. was supported by NSF IGERT Fellowship Award No. 0801471.

[1] Z. H. Stachurski, On structure and properties of amorphous materials, Materials **4**, 1564 (2011).
[2] N. Xu and C. S. O'Hern, Measurements of the yield stress in frictionless granular systems, Phys. Rev. E **73**, 061303 (2006).
[3] S. P. Das, *Statistical Physics of Liquids at Freezing and Beyond* (Cambridge University Press, Cambridge, 2011).
[4] M. L. Falk and J. S. Langer, Deformation and failure of amorphous, solidlike materials, Annu. Rev. Condens. Matter Phys. **2**, 353 (2011).
[5] E. Bouchbinder and J. S. Langer, Nonequilibrium thermodynamics of driven amorphous materials. I. internal degrees of freedom and volume deformation, Phys. Rev. E **80**, 031131 (2009).
[6] E. Bouchbinder and J. S. Langer, Nonequilibrium thermodynamics of driven amorphous materials. II. effective-temperature theory, Phys. Rev. E **80**, 031132 (2009).
[7] E. Bouchbinder and J. S. Langer, Nonequilibrium thermodynamics of driven amorphous materials. III. Shear-transformation-zone plasticity, Phys. Rev. E **80**, 031133 (2009).
[8] L. Boué, H. G. E. Hentschel, I. Procaccia, I. Regev, and J. Zylberg, Effective temperature in elastoplasticity of amorphous solids, Phys. Rev. B **81**, 100201 (2010).
[9] A. Argon and H. Kuo, Plastic flow in a disordered bubble raft (an analog of a metallic glass), Mater. Sci. Eng. **39**, 101 (1979).
[10] A. Argon, Plastic deformation in metallic glasses, Acta Metall. **27**, 47 (1979).
[11] F. Spaepen, A microscopic mechanism for steady state inhomogeneous flow in metallic glasses, Acta Metall. **25**, 407 (1977).
[12] D. Turnbull and M. H. Cohen, On the free-volume model of the liquid-glass transition, J. Chem. Phys. **52**, 3038 (1970).
[13] D. Srolovitz, V. Vitek, and T. Egami, An atomistic study of deformation of amorphous metals, Acta Metall. **31**, 335 (1983).
[14] D. Deng, A. S. Argon, and S. Yip, A molecular dynamics model of melting and glass transition in an idealized two-dimensional material. I. Phil. Trans. R. Soc. Lond. A **329**, 549 (1989).
[15] M. L. Falk and J. S. Langer, Dynamics of viscoplastic deformation in amorphous solids, Phys. Rev. E **57**, 7192 (1998).
[16] J. Ding, S. Patinet, M. L. Falk, Y. Cheng, and E. Ma, Soft spots and their structural signature in a metallic glass, Proc. Natl. Acad. Sci. **111**, 14052 (2014).
[17] V. V. Bulatov and A. S. Argon, A stochastic model for continuum elastoplastic behavior. I. numerical approach and strain localization, Simul. Mater. Sci. Eng. **2**, 167 (1994).
[18] G. Picard, A. Ajdari, F. Lequeux, and L. Bocquet, Slow flows of yield stress fluids: Complex spatiotemporal behavior within a simple elastoplastic model, Phys. Rev. E **71**, 010501 (2005).
[19] C. E. Maloney and A. Lemaître, Amorphous systems in athermal, quasistatic shear, Phys. Rev. E **74**, 016118 (2006).
[20] K. M. Salerno, C. E. Maloney, and M. O. Robbins, Avalanches in Strained Amorphous Solids: Does Inertia Destroy Critical Behavior? Phys. Rev. Lett. **109**, 105703 (2012).
[21] V. Mansard, P. Chaudhuri, L. Bocquet, and A. Colin, A kinetic elastoplastic model exhibiting viscosity bifurcation in soft glassy materials, Soft Matter **7**, 5524 (2011).
[22] R. Dasgupta, H. G. E. Hentschel, and I. Procaccia, Microscopic Mechanism of Shear Bands in Amorphous Solids, Phys. Rev. Lett. **109**, 255502 (2012).

[23] A. Lindsay Greer, Metallic glasses on the threshold, Mater. Today **12**, 14 (2009).

[24] H. Guo, J. Wen, N. M. Xiao, Z. F. Zhang, and M. L. Sui, The more shearing, the thicker shear band and heat-affected zone in bulk metallic glass, J. Mater. Res. **23**, 2133 (2008).

[25] L. Yao and Y. Luan, Evolution of shear banding flows in metallic glasses characterized by molecular dynamics, J. Appl. Phys. **119**, 234303 (2016).

[26] J. Luo, Y. Shi, and C. R. Picu, Shear-induced volumetric strain in CuZr metallic glass, Int. J. Eng. Sci. **83**, 99 (2014).

[27] A. L. Greer, Shear bands in metallic glasses, Mater. Sci. Eng. R-Rep. **74**, 71 (2013).

[28] L. Pechenik, Dynamics of shear-transformation zones in amorphous plasticity: Nonlinear theory at low temperatures, Phys. Rev. E **72**, 021507 (2005).

[29] J. S. Langer and L. Pechenik, Dynamics of shear-transformation zones in amorphous plasticity: Energetic constraints in a minimal theory, Phys. Rev. E **68**, 061507 (2003).

[30] A. Q. Tool, Relation between inelastic deformability and thermal expansion of glass in its annealing range, J. Amer. Ceram. Soc. **29**, 240 (1946).

[31] D. Turnbull and M. H. Cohen, Molecular transport in liquids and glasses, J. Chem. Phys. **31**, 1164 (1959).

[32] Th. M. Nieuwenhuizen, Ehrenfest Relations at the Glass Transition: Solution to an Old Paradox, Phys. Rev. Lett. **79**, 1317 (1997).

[33] Th. M. Nieuwenhuizen, Thermodynamics of the Glassy State: Effective Temperature as an Additional System Parameter, Phys. Rev. Lett. **80**, 5580 (1998).

[34] Th. M. Nieuwenhuizen, Thermodynamic picture of the glassy state gained from exactly solvable models, Phys. Rev. E **61**, 267 (2000).

[35] F. Sciortino, W. Kob, and P. Tartaglia, Inherent Structure Entropy of Supercooled Liquids, Phys. Rev. Lett. **83**, 3214 (1999).

[36] F. Sciortino and P. Tartaglia, Extension of the Fluctuation-Dissipation Theorem to the Physical Aging of a Model Glass-Forming Liquid, Phys. Rev. Lett. **86**, 107 (2001).

[37] E. La Nave, F. Sciortino, P. Tartaglia, M. S. Shell, and P. G. Debenedetti, Test of nonequilibrium thermodynamics in glassy systems: The soft-sphere case, Phys. Rev. E **68**, 032103 (2003).

[38] J. S. Langer, Dynamics of shear-transformation zones in amorphous plasticity: Formulation in terms of an effective disorder temperature, Phys. Rev. E **70**, 041502 (2004).

[39] W. J. Drugan and J. R. Willis, A micromechanics-based nonlocal constitutive equation and estimates of representative volume element size for elastic composites, J. Mech. Phys. Solids **44**, 497 (1996).

[40] J. L. Chaboche, A review of some plasticity and viscoplasticity constitutive theories, Int. J. Plastic. **24**, 1642 (2008).

[41] W. A. Curtin and R. E. Miller, Atomistic-continuum coupling in computational materials science, Modeling Simul. Mater. Sci. Eng. **11**, 33 (2003).

[42] P. Derosa, *Multiscale Modeling: From Atoms to Devices* (Taylor and Francis Group, Boca Raton, 2011).

[43] M. Dijkstra, R. van Roij, and R. Evans, Phase diagram of highly asymmetric binary hard-sphere mixtures, Phys. Rev. E **59**, 5744 (1999).

[44] P. G. Bolhuis, A. A. Louis, and J. P. Hansen, Shear-induced volumetric strain in CuZr metallic glass, Phys. Rev. E **64**, 021801 (2001).

[45] V. Bulatov and A. Argon, Stochastic model for continuum elasto-plastic behavior. III. plasticity in ordered versus disordered solids, Simul. Mater. Sci. Eng. **2**, 203 (1994).

[46] E. R. Homer and C. A. Schuh, Mesoscale modeling of amorphous metals by shear transformation zone dynamics, Acta Mater. **57**, 2823 (2009).

[47] E. R. Homer and C. A. Schuh, Three-dimensional shear transformation zone dynamics model for amorphous metals, Model. Simul. Mater. Sci. Eng. **18**, 065009 (2010).

[48] J. C. Baret, D. Vandembroucq, and S. Roux, Extremal Model for Amorphous Media Plasticity, Phys. Rev. Lett. **89**, 195506 (2002).

[49] M. Talamali, V. Petaja, D. Vandembroucq, and S. Roux, Avalanches, precursors and finite size fluctuations in a mesoscopic model of amorphous plasticity, Phys. Rev. E **84**, 016115 (2011).

[50] D. Vandembroucq and S. Roux, Mechanical noise dependent aging and shear banding behavior of a mesoscopic model of amorphous plasticity, Phys. Rev. B **84**, 134210 (2011).

[51] M. Talamali, V. Petaejae, D. Vandembroucq, and S. Roux, Strain localization and anisotropic correlations in a mesoscopic model of amorphous plasticity, Comptes Rendus Mec. **340**, 275 (2012).

[52] P. de Hey, J. Sietsma, and A. van den Beukel, Structural disordering in amorphous $pd_{40}ni_{40}p_{20}$ induced by high temperature deformation, Acta Mater. **46**, 5873 (1998).

[53] Y. Shi, M. B. Katz, H. Li, and M. L. Falk, Evaluation of the Disorder Temperature and Free-Volume Formalisms Via Simulations of Shear Banding in Amorphous Solids, Phys. Rev. Lett. **98**, 185505 (2007).

[54] S. Plimpton, Fast parallel algorithms for short-range molecular dynamics, J. Comp. Phys. **117**, 1 (1995).

[55] Y. Q. Cheng, E. Ma, and H. W. Sheng, Atomic-Level Structure of Multicomponent Bulk Metallic Glasses, Phys. Rev. Lett. **102**, 245501 (2009).

[56] D. J. Evans and G. P. Morriss, Nonlinear-response theory for steady planar couette flow, Phys. Rev. A **30**, 1528 (1984).

[57] The net (global) strain γ is the total shear strain due to the imposed velocity at the boundary of the simulation box. It is equivalent to the sum of the shear components of the strain tensor, namely $\gamma = 2\epsilon_{12}$.

[58] E. Dieterich, J. Camunas-Soler, M. Ribezzi-Crivellari, U. Seifert, and F. Ritort, Single-molecule measurement of the effective temperature in non-equilibrium steady states, Nat. Phys. **11**, 971 (2015).

[59] E. G. Daub, D. Klaumünzer, and J. F. Löffler, Effective temperature dynamics of shear bands in metallic glasses, Phys. Rev. E **90**, 062405 (2014).

[60] E. Bouchbinder, J. S. Langer, and I. Procaccia, Athermal shear-transformation-zone theory of amorphous plastic deformation. I. Basic rinciples, Phys. Rev. E **75**, 036107 (2007).

[61] E. Bouchbinder, J. S. Langer, and I. Procaccia, Athermal shear-transformation-zone theory of amorphous plastic deformation. II. Analysis of simulated amorphous silicon, Phys. Rev. E **75**, 036108 (2007).

[62] M. L. Manning, J. S. Langer, and J. M. Carlson, Strain localization in a shear transformation zone model for amorphous solids, Phys. Rev. E **76**, 056106 (2007).

[63] R. L. Moorcroft and S. M. Fielding, Criteria for Shear Banding in Time-Dependent Flows of Complex Fluids, Phys. Rev. Lett. **110**, 086001 (2013).

[64] M. L. Manning, E. G. Daub, J. S. Langer, and J. M. Carlson, Rate-dependent shear bands in a shear-transformation-zone model of amorphous solids, Phys. Rev. E **79**, 016110 (2009).

[65] J. S. Langer and M. L. Manning, Steady-state, effective-temperature dynamics in a glassy material, Phys. Rev. E **76**, 056107 (2007).

[66] C. H. Rycroft, Y. Sui, and E. Bouchbinder, An eulerian projection method for quasistatic elastoplasticity, J. Comp. Phys. **300**, 136 (2015).

[67] C. H. Rycroft and F. Gibou, Simulations of a stretching bar using a plasticity model from the shear transformation zone theory, J. Comp. Phys. **231**, 2155 (2012).

[68] Y. Q. Cheng, H. W. Sheng, and E. Ma, Relationship between structure, dynamics, and mechanical properties in metallic glass-forming alloys, Phys. Rev. B **78**, 014207 (2008).

[69] R. Maaß, D. Klaumünzer, and J. F. Löffler, Propagation dynamics of individual shear bands during inhomogeneous flow in a zr-based bulk metallic glass, Acta Mater. **59**, 3205 (2011).